HHS Public Access

Author manuscript

Magn Reson Med. Author manuscript; available in PMC 2020 June 01.

Published in final edited form as:

Magn Reson Med. 2019 June ; 81(6): 3440–3452. doi:10.1002/mrm.27686.

Modular ^{31}P Wideband Inversion Transfer for Integrative Analysis of ATP Metabolism, T_1 Relaxation and Molecular Dynamics in Skeletal Muscle at 7T

Jimin Ren[a,b,*], **A. Dean Sherry**[a,b,c], and **Craig R. Malloy**[a,b,d,e]

[a]Advanced Imaging Research Center, University of Texas Southwestern Medical Center, Dallas, TX 75390.

[b]Department of Radiology, University of Texas Southwestern Medical Center, Dallas, TX 75390.

[c]Department of Chemistry, University of Texas at Dallas, Richardson, TX 75080.

[d]Department of Internal Medicine, University of Texas Southwestern Medical Center, Dallas, TX 75390.

[e]VA North Texas Health Care System, Dallas, TX 75216.

Abstract

Purpose: For efficient and integrative analysis of de novo ATP synthesis, creatine kinase-mediated ATP synthesis, T_1 relaxation time and ATP molecular motion dynamics in human skeletal muscle at rest.

Methods: Four inversion-transfer modules differing in center inversion frequency were combined to generate amplified MT effects in targeted MT pathways including Pi ↔ γ-ATP, PCr ↔ γ-ATP and $^{31}P_{\gamma(\alpha)ATP}$ ↔ $^{31}P_{\beta ATP}$. MT effects from both forward and reverse exchange kinetic pathways were acquired to reduce potential bias and confounding factors in integrated data analysis.

Results: Kinetic data collected using four wideband inversion modules (8 min each) yielded the forward exchange rate constants $k_{PCr\rightarrow\gamma ATP} = 0.31 \pm 0.05\ s^{-1}$ and $k_{Pi\rightarrow\gamma ATP} = 0.064 \pm 0.012\ s^{-1}$, and the reverse exchange rate constants $k_{\gamma ATP\rightarrow Pi} = 0.034 \pm 0.006\ s^{-1}$ and $k_{\gamma ATP\rightarrow PCr} = 1.37 \pm 0.22\ s^{-1}$, respectively. The cross-relaxation rate constant $\sigma_{\gamma(\alpha)\leftrightarrow\beta ATP}$ was $-0.20 \pm 0.03\ s^{-1}$, corresponding to ATP rotational correlation time τ_c of $0.8 \pm 0.1 \times 10^{-7}$ s. The intrinsic T_1 relaxation times were Pi (9.2 ± 1.4 s), PCr (6.2 ± 0.4 s), γ-ATP (1.8 ± 0.1 s), α-ATP (1.4 ± 0.1 s), and β-ATP (1.1 ± 0.1 s). Muscle ATP T_1 values were found to be significantly longer than those previously measured in brain using similar method.

Conclusion: A combination of multiple inversion-transfer modules provides a comprehensive and integrated analysis of ATP metabolism and molecular motion dynamics. This relatively fast technique could be potentially useful for studying metabolic disorders in skeletal muscle.

[*]To whom correspondence should be addressed: Jimin Ren, PhD, 5323 Harry Hines Blvd, NE4.2, Dallas, Texas 75390-8568, (214) 645-2723, jimin.ren@utsouthwestern.edu.

Keywords

31P MRS; skeletal muscle; magnetization transfer; relaxation time; brain; ATP

Introduction

Skeletal muscle depends upon continuous production of ATP to fuel myofiber contraction (1). Even in the resting state, skeletal muscle consumes ATP at a basal metabolic rate necessary to maintain essential cellular activities and keep the muscle prepared for rapid transition to exercise during which energy expenditure could increase a hundredfold (2). Since skeletal muscle at rest derives its ATP energy mainly through mitochondrial oxidation rather than cytosolic glycolysis, it is natural to consider impaired ATP synthesis in resting muscle to be a potential biomarker of mitochondrial dysfunction which may occur under compromised metabolic conditions such as aging, insulin resistance and type 2 diabetes (3–11). However, Kemp noted that the Pi → ATP flux measured with ^{31}P saturation transfer (ST) has no straightforward relationship with metabolic capacity or mitochondrial function (12,13).

The inconsistency and considerable variations in ATP synthesis rate measured using different methods complicate the ST data interpretation (11–16). It is speculated the prolonged RF irradiation and other technical issues may cause unintended artifacts in the measurements of ATP synthesis by ST (4,17–20). In recent years, various alternative inversion transfer (IT) methods have been developed (21–27). Unlike ST methods, inversion transfer (IT) is based on a short inversion pulse, which can induce MT effects in post-inversion period after the RF pulse is completely turned off, thus free of typical ST-related artifacts. IT has multiple additional advantages. First, the short MT preparation pulse is easy to implement on any MRI scanners with multinuclear capabilities. Second, IT is efficient because the inverted magnetization enjoys a larger dynamic range, theoretically from $-M^{\circ}$ to M°. Third, the kinetic and T_1 parameters can be evaluated simultaneously without the need for a separate time-consuming saturation-controlled T_1 experiment as required by steady-state ST (4). Finally, in an IT experiment, the evolution of post-pulsing magnetization can be described solely by Mz-terms, independent of pulsing conditions, making IT suitable for integrated analysis of large spin systems involving multiple co-existent MT pathways (Figure 1a).

While a complex ^{31}P exchange system contains rich information about various ATP kinetics related to metabolism and molecular motional dynamics, it poses a practical challenge in measuring slow de novo ATP synthesis. In resting skeletal muscle, the flux by reaction Pi → γ-ATP is one order of magnitude smaller than that by co-existent CK-mediated reaction PCr → γ-ATP (Figure 1A), making classical narrow-band inversion measurement inefficient due to MT competitions. A novel strategy to cope with slow Pi → γ-ATP exchange kinetics is to use wideband-based inversion, which is based on simultaneous inversion of γ-ATP together with PCr, α- and β-ATP. This creates a large buffer of polarized magnetization enable to replenish inverted γ-ATP pool against T_1 relaxation, thus prolonging the exchange time between γ-ATP and Pi and amplifying the MT effect at Pi (22–24). Exchange kinetics

by band inversion transfer (EBIT) has been proven to be particularly effective in amplifying the MT effects reflective of de novo ATP synthesis.

Recently we proposed the concept of modular EBIT (mEBIT) to measure MT effects in multiple coexistent MT pathways, with intent to fully extract the metabolic and molecular physics information embedded in the entire exchange system (26). An mEBIT approach would offer the advantage of acquisition flexibility and data integrity, since it allows each elected MT pathway probed by a specifically tailored module while the resultant datasets from different modules can be assembled for an integrated data analysis. A three-module mEBIT method has been demonstrated for assessment of both kinetic and relaxation rates in the human brain (26). In the current study we aim to explore the benefit of introducing a new module with unique feature of measuring MT effects in the reverse reaction pathways Pi ← γ-ATP and PCr ← γ-ATP (Module IV, Figure 1C). This new module is expected to bring in more balanced MT datasets to reduce potential bias and confounding factors in data analysis. An integrative study has recently been reported using a single wideband module (27), inclusion of Module IV in mEBIT fitting is expected to significantly improve the fitting variances. The current work is the first integrative study of ATP metabolism and T_1 relaxation in skeletal muscle using mEBIT approach.

Despite the fact that they share the same exchange mechanisms among Pi, PCr and ATP spins, skeletal muscle and brain differ markedly in both exchange kinetics and metabolite concentrations. For example, the rate constant of de novo ATP synthesis is typically 3- to 4-fold slower whereas the PCr/ATP concentration ratio is 3- to 4-fold larger in muscle compared to brain (21,23,25). This results in a much delayed transition in the biphasic exchange-relaxation recovery curve for Pi in muscle. For scan efficiency and measurement reliability mEBIT will be executed with short TR, with TR adjusted to optimally capture the kinetic features of muscle at rest. We will also compare the difference in ATP kinetics and T_1 relaxation between brain and skeletal muscle.

Methods

Human Subjects

The protocol was approved by the Institutional Review Board of the University of Texas Southwestern Medical Center. Prior to the MRS study, informed written consent was obtained from all participants. Seven subjects (2 male and 5 female), aged 26 ± 3 yr, BMI 21 ± 2, resting heart rate 71 ± 9, and peripheral capillary oxygen saturation (SpO_2) 98 ± 2%, participated in the study. All subjects were in good general health with no history of periphery or neuromuscular diseases, and were asked to refrain from any physical activity of moderate or higher intensity 24-hr prior to the study and to sit at rest for 20 min prior to the scan.

MRS Protocol

All subjects were positioned head-first and supine in the MRI scanner (7T Achieva, Philips Healthcare, Cleveland, OH), with calf muscle of the primary leg positioned in the center of the detection RF coil (Philips Healthcare, Cleveland, OH). The leg position was secured by

Velcro straps with a thick pad in between for cushion, and the subject were asked to keep still and not to make muscle excursions. The RF coil was a half-cylinder-shaped partial volume, double-tuned $^{1}H/^{31}P$ quadrature TR coil consisting of two tilted, partially overlapping 10 cm loops, with a solid base that can be firmly attached to the scanner table. Axial, coronal, and sagittal T2-weighted turbo spin echo images were acquired for shimming voxel planning. Second order ^{1}H-based automatic volume shimming was applied prior to ^{31}P spectral acquisitions.

All four mEBIT modules in the current study are summarized in Table 1. These four modules differ only in center frequency of inversion band (Figure 1C). The mEBIT pulse sequence was consisted of an adiabatic inversion pulse, followed by a variable delay time t_d, a hard 90° readout pulse, and a post-readout recovery period with constant TR = 7 s (Figure 1B). For each data series, a total of 7 delay times were sampled, they were spaced logarithmically, each with 8 scan averages, and preceded by one dummy scan. The first t_d point was 30 ms for all modules, while the last t_d was 3 s for Module III, 5 s for Modules I and IV; and 6 s for Module II. The data acquisition time was ~ 8 min for each module. The inversion pulse was a short trapezoid-shaped adiabatic pulse (pulse width pw = 38 ms, including 7 ms of pre- and post-ramp time) with a maximal B_1 of 13 μT.

In addition to acquiring mEBIT datasets with varying t_d, a reference scan was performed with TR = 7 s but without inversion. An additional fully relaxed ^{31}P spectrum was also acquired at TR = 30 s to measure the z-magnetization at thermal equilibrium ($M_z°$).

To evaluate mEBIT reproducibility in measurement of kinetic and T_1 relaxation, four of the seven subjects were scanned twice at two visits separated by 1–2 weeks but under the same experimental conditions and procedures.

Other common ^{31}P NMR parameters included sampling points 4 K, zero-filled to 8 K prior to FT, transmitter carrier frequency offset 50 Hz downfield from α-ATP signal. The chemical shifts of all ^{31}P metabolites were referenced to PCr at 0 ppm. Gaussian apodization was applied to each FID prior to Fourier transformation using the scanner software (SpectroView, Philips Healthcare).

^{31}P MRS Data Analysis

The frequency-domain ^{31}P spectra were baseline corrected, and the signal intensities for Pi, PCr, and α-, β- and γ-ATP were measured by peak area-under-curve (integral) and normalized by the corresponding signals in the reference spectrum to derive $m(t_d)$. To evaluate the parameters $k_{Pi\rightarrow\gamma ATP}$, $k_{PCr\rightarrow\gamma ATP}$, $\sigma_{\gamma(\alpha)\leftrightarrow\beta ATP}$, $T_{1,Pi}$, $T_{1,PCr}$, $T_{1,}$, $T_{1,}$ and $T_{1,}$, the $m(t_d)$ datasets were fitted by 5-pool model (Figure 1A) according to 4Equation [5] (Supplementary Information), based on least-square function *lsqcurvefit* in Matlab (The MathWorks, Inc. Natick, MA). The ATP rotation correlation time τ_c was derived from σ as described previously (25).

^{31}P MRS Data Simulation

The $m(\tau)$ data were simulated for Pi, PCr, and α-, β- and γ-ATP to show the dependence of $m(\tau)$ on the recovery time τ after a 90° readout pulse. The simulation was done according to the five-spin exchange model (Figure 1a) and Equations [1–5] (Supplementary Information), with τ varied in the range of 0 – 30 s. Other simulation parameters included: Pi/ATP = 0.54, PCr/ATP = 4.44, $k_{Pi\rightarrow\gamma ATP} = 0.06\ s^{-1}$, $k_{PCr\rightarrow\gamma ATP} = 0.30\ s^{-1}$, $\sigma = -0.19\ s^{-1}$, T_1 = 9.0, 6.0, 1.9, 1.4, and 1.1 s for Pi, PCr, γ-, α- and β-ATP, respectively, which were set in line with the corresponding fitting results in resting skeletal muscle. For comparison, simulated $m(\tau)$ datasets were also generated for the scenario in the absence of MT effect assuming $k_{Pi\rightarrow\gamma ATP} = k_{PCr\rightarrow\gamma ATP} = \sigma = 0$.

Statistical Analysis

All data are reported as mean ± standard deviation, calculated using Matlab. The ^{31}P T_1, and forward and reverse rate constants were compared between brain (26) and skeletal muscle using unpaired t-test function *ttest2*, with $p < 0.05$ indicating statistically significant difference.

Results

Data Simulation

Figure 2 shows the simulated data for the normalized z-magnetization, $m(\tau)$, against recovery time τ, for the five-spin exchange system composed of Pi, PCr, α-, β- and γ-ATP. A comparison between presence ($k \neq 0$ and $\sigma \neq 0$) and absence ($k = \sigma = 0$) of MT reveals that MT greatly speeds up the magnetization recovery of long-T_1 spins (Pi and PCr) while MT significantly slows down the recovery of short T_1-spin (γ-ATP). Figure 2D plots the curves of $|\Delta m(\tau)|$, the magnetization difference between presence and absence of MT, for Pi, PCr and γ-ATP which are involved in ATPase- and CK-mediated exchange reactions. The $|\Delta m(\tau)|$ curve yields a maximum at a τ value of 11.6 s, 6.5 s, and 3.0 s for Pi, PCr and γ-ATP, respectively. Their average (= 7.0 s) was chosen as TR in the current mEBIT study.

Compared to acquisition for a fully relaxed spectrum with long TR of 30 sec and scan average NA = 1, the acquisition for a partially relaxed spectrum with short TR of 7 s and NA =4 would increase SNR by an average of 3.2-fold (Pi, 2.4; PCr, 3.0; α-, β- and γ-ATP; 3.8, 3.7 and 3.2) in skeletal muscle (Figure 2C).

mEBIT Modules

a) Module I and II—The primary intent of these two modules was to measure MT effects in the forward ATP synthesis reactions Pi → γ-ATP and PCr → γ-ATP. In module I, all three ATP spins were inverted, while in Module II, PCr was also co-inverted. Module I generated a MT effect of 10% at both Pi and PCr (Figure 3A, 3E and 3I). In comparison, Module II yielded a larger MT effect of 16% at Pi (Figure 3B and3F).

b) Module III—Module-III was intended to maximize MT effect at β-ATP by activating two parallel cross-relaxation pathways ($^{31}P_\alpha$ - $^{31}P_\beta$ and $^{31}P_\beta$ - $^{31}P\gamma$) within ATP. The co-

inversion of Pi, PCr with α- and γ-ATP led to a large maximal MT effect of 25% at β-ATP, which occurred at t_d ~ 1.3 s (Figure 3C and 3G).

c) Module IV—In contrast to Modules I and II, Module IV was intended to elicit MT effects in the reverse reactions γ-ATP → Pi and γ-ATP → PCr. The co-inversion of Pi and PCr led to a striking large MT effect of 49% at γ-ATP, occurred at t_d ~ 0.9 s (Figure 3D and3H). This direct MT effect was so large that a relayed MT effect of 14% was also clearly observed at β-ATP (Figure 3J). No further MT effect was measureable at α-ATP.

Data Fitting

To evaluate the kinetic and relaxation parameters, the $m(t_d)$ versus t_d datasets from all four mEBIT modules were fitted together according to the 5-spin exchange model (Figure 4). The fitting which included a total of 160 data points in 20 $m(t_d)$ datasets (160 = 5 spins x 4 modules x 8 time points), yielded the following kinetic rate constants and relaxation times : $k_{PCr\rightarrow\gamma ATP}$ 0.31 ± 0.05 s^{-1}, $k_{Pi\rightarrow\gamma ATP}$ 0.064 ± 0.012 s^{-1}, $\sigma_{\gamma(\alpha)\leftrightarrow\beta ATP}$ - 0.20 ± 0.03 s^{-1}, correspond to ATP rotation correlation time τ_c (0.8 ± 0.1) $\cdot 10^{-7}$ s, and T_1 relaxation times Pi 9.2 ± 1.4 s, PCr 6.2 ± 0.4 s, γ-ATP 1.8 ± 0.1 s, α-ATP 1.4 ± 0.1 s, and β-ATP 1.1 ± 0.1 s (n = 7, Table 2, Figure 5). The reverse exchange rate constants were 0.034 ± 0.006 s^{-1} for $k_{\gamma ATP\rightarrow Pi}$ (= $k_{Pi\rightarrow\gamma ATP}$ [Pi] / [ATP]) and 1.37 ± 0.22 s^{-1} for $k_{\gamma ATP\rightarrow PCr}$ (= $k_{PCr\rightarrow\gamma ATP}$ [PCr] / [ATP]), respectively (Figure 6).

Given potential interdependence among $m(t_d)$ datasets of different modules, data fittings were also performed with inclusion of fewer mEBIT modules to explore optimal module combinations that could lead to more efficient scans with acceptable outcomes. Table 2 summarizes the results of several selected modular combinations including 1) two-module combination: Modules I & IV; and 2) three-module combinations: Modules I, II & III and Modules I, II & IV. To test the feasibility of evaluating de novo ATP synthesis (Pi → γ-ATP) using minimal $m(t_d)$ datasets, a data fitting was also conducted using just two datasets acquired for Pi and γ-ATP by Module II, based on a simplified two-spin exchange model.

Intra-subject Variability

To evaluate mEBIT reproducibility in measuring kinetic and T_1 relaxation parameters, four of the seven subjects were scanned twice at two visits separated by 1–2 weeks but under the same experimental conditions and procedures. The intra-subject variations evaluated by four module combination were $k_{PCr\rightarrow\gamma ATP}$ 13 ± 9 %, $k_{Pi\rightarrow\gamma ATP}$ 14 ± 8 %, $\sigma_{\gamma(\alpha)\leftrightarrow\beta ATP}$ 8 ± 2 %, T_1 (Pi) 9 ± 6 %, T_1 (PCr) 5 ± 1 %, T_1 (γ-ATP) 2 ± 1 %, T_1 (α-ATP) 2 ± 1 %, and T_1 (β-ATP) 3 ± 2 %, respectively.

Discussion

It has been technically challenging to measure in vivo ATP metabolism in an efficient and integrative manner in humans using ^{31}P NMR and various magnetization transfer techniques. This is especially true in resting skeletal muscle where the rate of de novo ATP synthesis is exceptionally slow (0.064 ± 0.012 s^{-1}, Table 1) in comparison to the magnitude of other rate constants involved in the exchange system including T_1 relaxation of γ-ATP

and Pi (T_1^{-1}: 0.54 ± 0.02 and 0.11 ± 0.02 s^{-1}), ATP intramolecular cross-relaxation (0.20 ± 0.03 s^{-1}) and phosphoryl exchange between PCr and γ-ATP (0.31 ± 0.05 s^{-1}). In the current study, we used a short-TR, modular EBIT approach (mEBIT) for efficient and integrative evaluation of kinetic and relaxation properties of the entire ^{31}P exchange system in human muscle at 7T.

As shown in Figures 3 and 4, all mEBIT modules clearly illustrated the "fall-rise" biphasic pattern in $m(t_d)$ curves characteristic of a typical inversion transfer experiment. The quantitative outcomes were highly reproducible as indicated by the small intra-subject variances evaluated between two visits separated by 1–2 weeks (< 15% for $k_{PCr\rightarrow\gamma ATP}$ and $k_{Pi\rightarrow\gamma ATP}$; < 10% for $\sigma_{\gamma(\alpha)\leftrightarrow\beta ATP}$ and T_1 of Pi and PCr, and < 5% for T_1 of ATP spins). While wideband inversion elicits larger MT effects as compared to the narrow-band approach, the magnitude of direct MT effect induced by the new mEBIT module (Model IV) is by far the largest (45% at γ-ATP). This new module also creates a substantial relayed MT effect (14% at β-ATP) through extended pathway PCr ↔ γ-ATP ↔ β-ATP. Without direct RF perturbing at γ-ATP, the appearance of MT effect in γ-ATP ↔ β-ATP pathway provides strong evidence for presence of intramolecular NOE effect within ATP in vivo.

Theoretical analysis indicates that, for a large spin-system inter-connected by multiple coexistent MT pathways, any perturbation in one spin will affect the state of all other spins in the system, as governed by the kinetic and relaxation properties that define the system. The question is how to design proper perturbation schemes to elicit the largest possible system responses so that one can reliably and efficiently derive these governing parameters with minimal bias. In the current study, we used multiple modules to acquire $m(t_d)$ datasets for each and every MT pathways in both forward and reverse reactions. With a large assembly of $m(t_d)$ datasets, potential measurement bias and confounding factors among different fitting parameters are expected to be minimized.

A main challenge in a large system is that MT effect in a given pathway can be greatly reduced due to competition from other coexistent MT pathways. mEBIT was implemented to break down this barrier, by synergizing magnetizations in otherwise competitive pathways to stimulate the largest possible MT effect in a selected pathway, whereby making the derived MT effect suitable for assessing metabolic information. Among the four modules studied, Module II targets Pi → γ-ATP pathway for evaluation of de novo ATP synthesis by co-inverting PCr with all ATP spins; Module III measures ATP intramolecular cross-relaxation or NOE effect (γ- ↔ β-ATP and α- ↔ β-ATP) by co-inverting Pi, PCr, γ- and α-ATP. Modules I and IV together stimulate both forward and reverse CK-mediated exchanges (PCr ↔ γ-ATP), respectively. These latter two modules are also able to acquire additional MT information about the Pi → γ-ATP pathway and γ- ↔ β-ATP pathways, respectively (Figure 3). This was achieved by shifting the center inversion frequency closer to PCr (by Module I) and γ-ATP (by Module IV), so that the resultant partial saturation of PCr (by Module I) and γ-ATP (by Module IV) inhibits the MT competition from CK pathway (PCr ↔ γ-ATP) and consequently promotes the MT effect at Pi (Module I) and β-ATP (Module IV).

Module II is of particular importance in the evaluation of de novo ATP synthesis (Pi → γ-ATP). By co-inversion of PCr and γ-ATP, Module-II generated a maximal MT effect of 16% at Pi (Figure 3). Module-II alone yielded a reasonable $k_{Pi \rightarrow \gamma ATP}$ value of 0.083 ± 0.022 s^{-1}, as compared to the results from multiple module fittings (= 0.065 ± 0.014 s^{-1} by Modules I, II & III, 0.067 ± 0.015 s^{-1} by Modules I, II & IV, and 0.064 ± 0.012 s^{-1} by Modules I-IV, Table 2). Given the short modular scan time (~ 8 min) and simplicity of involving only Pi and γ-ATP for deriving $k_{Pi \rightarrow \gamma ATP}$, Module II could be adopted when one needs to assess $k_{Pi \rightarrow \gamma ATP}$ while the available scan time is limited.

For a simple A ↔ B exchange system, empirical knowledge tells that to reliably measure the rate constant of the exchange, one should measure MT effects in both ways, A → B and A ← B, to reduce experimental bias. Modular band inversion (mEBIT) allows such concept to be carried out so balanced $m(t_d)$ datasets can be acquired, this is because MT effects in forward and reverse reactions can be separately probed in two different modules. A combination of resultant $m(t_d)$ datasets is expected to reduce fitting bias in analysis of kinetic and relaxation parameters (k, σ, and T_1). Modules I & IV are such a pair of modules complementary to each other: In Module I, α-, β-, and γ-ATP were inverted spins while Pi and PCr were un-inverted, whereas the opposite was true in Module IV. Together these two complementary modules yielded a good estimate for both $k_{Pi \rightarrow \gamma ATP}$ and $k_{PCr \rightarrow \gamma ATP}$ values (0.060 ± 0.026 and 0.33 ± 0.04 s^{-1}, Table 2), reflective the positive role of bi-directional constraints in data fitting of MT effects in two-way exchange reactions (Pi ↔ γ-ATP and PCr ↔ γ-ATP).

Further improvement in data fitting is expected when data from more modules are combined, as indicated by the results from a combination of Modules I, II & III (Table 2). The resultant Pi → γ-ATP rate constant (0.064 ± 0.012 s^{-1}) from this combination agrees well to previous results obtained in resting calf muscle of lean heathy subjects using long-TR EBIT by our group ($k_{Pi \rightarrow \gamma ATP}$ = 0.073 ± 0.011 s^{-1}, n = 10, BMI = 24 ± 2, age = 28 ± 4; $k_{Pi \rightarrow \gamma ATP}$ = 0.066± 0.017 s^{-1}, n = 14, BMI = 24 ± 2, age = 27 ± 4 (22,23), and using ST by others ($k_{Pi \rightarrow \gamma ATP}$ = 0.057 ± 0.012 s^{-1} (gastrocnemius) and 0.059 ± 0.012 s^{-1} (soleus), n = 5 (4); $k_{Pi \rightarrow \gamma ATP}$ = 0.068 ± 0.003 s^{-1}, n = 7, BMI = 22.9 ± 1.7, age = 28 ± 2 (ref (28) with unit correction). A somewhat large $k_{Pi \rightarrow \gamma ATP}$ value was also reported using ST (for example, 0.12 ± 0.01 s^{-1} n = 8, ref(29)).

It is believed that ATP synthesis in skeletal muscle occurs mainly in mitochondria through F1F0-ATPase and that the contribution from glycolysis pathway is not significant under normal physiology. Measurements from mEBIT and other MT-based methods that do not depend on perturbing cellular concentrations of ATP, PCr, Pi, ADP and H^+, may reflect the basal ATP production necessary for essential cellular processes. In contrast, the alternative post-exercise PCr recovery method measures “net” ATP production in muscle after the metabolic state is disturbed (see Broek et al (14), and Prompers et al (30)). Note that the dynamic PCr recovery approach does not detect a subset of ATP production that is consumed during the process of muscle recovery after exercise. Perhaps “net” or suprabasal ATP synthesis may be closely related to mitochondrial fitness − the capability to restore an acutely disturbed metabolic state. In this sense, post-exercise PCr recovery and mEBIT are

complementary in offering an integrated view of cellular bioenergetics in vivo, both reporting cellular ATP production but from different perspectives.

With mEBIT, the forward kinetic exchange rate constant for CK reaction ($k_{PCr\rightarrow \gamma\text{-ATP}}$) was 0.31 ± 0.05 s^{-1} (Module I - IV), which is in agreement with findings by other groups. For example, a same value (0.31 ± 0.05 s^{-1}, n=9) was reported by Parasoglou et al (31) in gastrocnemius muscle using continuous ST and IR T_1 measurement. Using four-angle-saturation-transfer (FAST) method, Bottomley et al (32) obtained a $k_{PCr\rightarrow \gamma\text{-ATP}}$ value of 0.29 ± 0.06 s^{-1} (n = 10, 1.5T). Other laboratories also reported similar results (0.26 ± 0.06 s^{-1} in gastrocnemius muscle at 7T by Jelenc et al (29); 0.25 ± 0.05 s^{-1} in vastus muscle at 3T by Pouymayou et al (27); 0.30 ± 0.06 s^{-1} in soleus, 0.27 ± 0.06 s^{-1} in gastrocnemius, and 0.35 ± 0.03 s^{-1} in calf muscle at 7T by Valkovic et al (33, 34)). The results in Table 2 indicate that inclusion of Module IV in mEBIT fitting reduces relative variance in $k_{PCr\rightarrow \gamma\text{-ATP}}$ (Δk/k: 12.1 % Module I & IV; 12.5% Module I, II & IV, and 16.1% Module I, II & III).

The rate constant (σ) for ATP cross-relaxation (NOE effect) was −0.20 ± 0.03 s^{-1} by four-module combination (assuming $\sigma_{\alpha \leftrightarrow \beta ATP} = \sigma_{\gamma \leftrightarrow \beta ATP}$), which is in reasonable agreement with our previous results by EKIT (21). Module III, which targets NOE effects, played a crucial role in σ evaluation, as evidenced by the smaller σ variation when Module III was included compared to results without Module III (Table 2). The variation in σ is significantly reduced with mEBIT as compared to a recent report using a single wideband inversion module ($\sigma_{\gamma \leftrightarrow \beta ATP}$:−0.32 ± 0.10 s^{-1} and $\sigma_{\alpha \leftrightarrow \beta ATP:}$ −1.00 ± 0.69 s^{-1}, ref(27) with unit correction), highlighting the importance of multiple-module approach in integrated data analysis.

One can design more modules to further improve fitting reliability. However, the incremental value in improvement tends to reduce as more modules are added, due to proportional increase in scan time and potential redundancy in constraints.. The results in Table 2 suggests that a three-module approach (Modules I, II & III) is a good substitute for four-module approach (Module I-IV) with balanced scan efficiency and fitting reliability in both k and σ. In case of scan restraints, mEBIT has the flexibility to allow fewer modules used for integrated data analysis.

For multiple module approach, TR is also a key factor affecting scan efficiency and fitting reliability. Scan efficiency tends to decrease if TR is too long, whereas fitting reliability would compromise if TR is too short to fairly capture the kinetic information among spins of interest. In the current study, TR was “optimized” by maximizing the difference in m between presence and absence of kinetic exchanges with equal weighting (Figure 2D). A TR of 7 s was selected as an average found for Pi, PCr and γ-ATP, as involved in the kinetic reactions Pi → γ-ATP and PCr → γ-ATP (Figure 1A).

A TR of 7 s for resting skeletal muscle is significantly longer than TR = 4 s previously used for a mEBIT study in human brain, which is consistent with the disparity in metabolic features between these two organs. As indicated in Figure 6, both the forward and reverse exchange rate constants for Pi ↔ γ-ATP are significantly slower in resting skeletal muscle

than in brain. Moreover, in brain, the ATP turnover rate in de novo ATP synthesis is ~10-fold slower than that in CK-mediated reaction γ-ATP → PCr, whereas the difference is 40-fold in resting skeletal muscle (assessed by $k_{\gamma ATP \rightarrow Pi}$ / $k_{\gamma ATP \rightarrow PCr}$ ratio, Figure 6). This also highlights the extraordinary technical challenges of measuring de novo ATP synthesis in resting human skeletal muscle as compared to brain. Note that, though $k_{\gamma ATP \rightarrow Pi}$ and $k_{\gamma ATP \rightarrow PCr}$ denote respectively the unidirectional rate constants for ATP breakdown reactions ATP → Pi + ADP and ATP + Cr → ADP + PCr, these two reverse exchange rate constants also represent concentration-independent, normalized ATP synthesis fluxes (catalyzed by ATPase and CK, respectively), because of relationship $k_{\gamma ATP \rightarrow Pi} = k_{Pi \rightarrow \gamma ATP}$ [Pi] / [ATP] and $k_{\gamma ATP \rightarrow PCr} = k_{PCr \rightarrow \gamma ATP}$ [PCr] / [ATP]) (Theory, Supplementary Information).

Interestingly, while brain and resting skeletal muscle have similar T_1 values for Pi and PCr (26), the T_1 values for ATP spins are significantly longer in muscle than those previously found in brain (Ren et al (26), Figure 5). Although the reason is not clear at present, it is speculate that there may be heterogeneity in oxygenation and metabolite distribution in different cellular compartments and tissues. The finding of much shorter ATP T_1's in brain than in resting muscle is consistent with the fact that the cerebral tissue is highly oxygenated (35) and that the endogenous O_2 can act as T_1-reducing agent. Additionally, the brain has a much higher ATP turnover rate catalyzed by ATPase (Figure 6), whereas ATPase activity is "oxygen-sensitive" (36) with major signaling molecules including oxygen-derived free radicals (36) which are also efficient T_1-shortening agents. It would be useful if ATP ^{31}P T_1 does report intracellular oxygenation for oxidative metabolism. Further exploratory work may be needed to establish this new role of ATP.

A limitation of the current study is that non-localized ^{31}P spectra were acquired with the use of a hard block pulse instead of an adiabatic half-passage pulse for excitation. The latter could yield a more uniform B1-insensitive excitation (Bottomley et al (31), 1.5T), while for muscle ^{31}P MRS at 7T, a high-B1 hard pulse is typically more advantageous in SNR, which is a desirable factor for the current mEBIT study that involves acquisition of many m(t_d) datasets within a short time period. Despite being un-localized, the observed 31P signals are predominantly contributed from soleus-gastrocnemius region with fair uniformity (Supporting Information Figure S1), attributable mainly to the performance of the half-cylinder-shaped partial volume RF coil used and the volume-based shimming. Moreover, with the use of 90° excitation, the resultant z-magnetization reaches steady state immediately after a single dynamic scan (taken as a dummy scan in the current study, Supporting Information Figure S2), which makes data analysis quite straightforward using the Z-magnetization expression (Equation [4], Supplementary Information). Alternatively, efficient data acquisition can be made by exciting with smaller flip angles using adiabatic pulse, as described in depth by Bottomley et al (31,37). Perhaps one could further improve spatial specificity using localized techniques and by taking into account of regional difference in fiber-type composition and Pi compartmental effects (38). A recent comparison study, however, found no significant difference in any of calculated kinetic parameters measured by the DRESS-localized FAST and non-localized standard ST (29), and no difference in $k_{Pi \rightarrow \gamma ATP}$ was found between fiber-composition different soleus and gastrocnemius muscles (4). While the current work is focused on skeletal muscle at rest, it is

possible that, with some modification, mEBIT may be adapted to exercising muscle; an elegant protocol has recently been reported by Sleigh et al (39) which allows ST measurement of ATP flux during muscle exercise, with an interesting observation of correlation between exercising ATP flux (above basal levels) and oxidative ATP synthesis measured from post-exercise PCr recovery (39).

In summary, we have demonstrated that the short-TR, modular wideband inversion transfer (mEBIT) approach can provide an efficient and integrative solution for evaluating ATP metabolism and basic NMR relaxation properties in resting skeletal muscle. With the potential link between impaired energy metabolism and deranged mitochondrial functions, mEBIT may serve as a valuable tool to advance our understanding of the role of ATP metabolism in onset and progression of various metabolic diseases (40–42).

Supplementary Material

Refer to Web version on PubMed Central for supplementary material.

ACKNOWLEDGEMENTS

The authors are grateful for technical assistance from Ivan Dimitrov and operational assistance from Salvador Pena. Jeannie Baxter and Janet Jerrow recruited and managed the human subjects. This project was supported by the National Center for Research Resources and the National Institute of Biomedical Imaging and Bioengineering of the National Institutes of Health through P41EB015908.

REFERENCES

1. Barclay CJ. Energy demand and supply in human skeletal muscle. J Muscle Res Cell Motil. 2017;38(2):143–155. [PubMed: 28286928]
2. Baker JS, Baker JS, McCormick MC, Robergs RA. Interaction among skeletal muscle metabolic energy systems during intense exercise. J Nutr Metab. 2010;2010:905612. [PubMed: 21188163]
3. Schrauwen-Hinderling VB, Roden M, Kooi ME, Hesselink MK, Schrauwen P. Muscular mitochondrial dysfunction and type 2 diabetes mellitus. Curr Opin Clin Nutr Metab Care. 2007;10(6):698–703. [PubMed: 18089950]
4. Befroy DE, Rothman DL, Petersen KF, Shulman GI. ^{31}P-magnetization transfer magnetic resonance spectroscopy measurements of in vivo metabolism. Diabetes. 2012; 61(11):2669–78. [PubMed: 23093656]
5. Petersen KF, Dufour S, Shulman GI. Decreased insulin-stimulated ATP synthesis and phosphate transport in muscle of insulin-resistant offspring of type 2 diabetic parents. PLoS Med. 2005;2(9):e233. [PubMed: 16089501]
6. Petersen KF, Befroy D, Dufour S, Dziura J, Ariyan C, Rothman DL, DiPietro L, Cline GW, Shulman GI Mitochondrial dysfunction in the elderly: possible role in insulin resistance. Science. 2003;300(5622):1140–2. [PubMed: 12750520]
7. Sleigh A, Raymond-Barker P, Thackray K, Porter D, Hatunic M, Vottero A, Burren C, Mitchell C, McIntyre M, Brage S, Carpenter TA, Murgatroyd PR, Brindle KM, Kemp GJ, O'Rahilly S, Semple RK, Savage DB. Mitochondrial dysfunction in patients with primary congenital insulin resistance. J Clin Invest. 2011;121(6):2457–61. [PubMed: 21555852]
8. Szendroedi J, Zwettler E, Schmid AI, Chmelik M, Pacini G, Kacerovsky G, Smekal G, Nowotny P, Wagner O, Schnack C, Schernthaner G, Klaushofer K, Roden M. Reduced basal ATP synthetic flux of skeletal muscle in patients with previous acromegaly. PLoS One. 2008;3(12):e3958. [PubMed: 19093000]
9. Affourtit C Mitochondrial involvement in skeletal muscle insulin resistance: A case of imbalanced bioenergetics. Biochim Biophys Acta. 2016;1857(10):1678–93. [PubMed: 27473535]

10. Holloszy JO. “Deficiency” of mitochondria in muscle does not cause insulin resistance. Diabetes. 2013;62(4):1036–40. [PubMed: 23520283]
11. Valkovič L, Ukropcová B, Chmelík M, Baláž M, Bogner W, Schmid AI, Frollo I, Zemková E, Klimeš I, Ukropec J, Trattnig S, Kršňák M. Interrelation of 31P-MRS metabolism measurements in resting and exercised quadriceps muscle of overweight-to-obese sedentary individuals. NMR Biomed. 2013;26(12):1714–22. [PubMed: 23949699]
12. Kemp GJ. The interpretation of abnormal 31P magnetic resonance saturation transfer measurements of Pi/ATP exchange in insulin-resistant skeletal muscle. Am J Physiol Endocrinol Metab. 2008;294(3):E640–2. [PubMed: 18325881]
13. Kemp GJ, Brindle KM. What do magnetic resonance-based measurements of Pi→ATP flux tell us about skeletal muscle metabolism? Diabetes. 2012 8;61(8):1927–34. [PubMed: 22826313]
14. van den Broek NM, Ciapaite J, Nicolay K, Prompers JJ. Comparison of in vivo postexercise phosphocreatine recovery and resting ATP synthesis flux for the assessment of skeletal muscle mitochondrial function. Am J Physiol Cell Physiol. 2010;299(5):C1136–43. [PubMed: 20668212]
15. Marcinek DJ. Mitochondrial dysfunction measured in vivo. Acta Physiol Scand. 2004;182(4):343–52. [PubMed: 15569095]
16. De Feyter HM, van den Broek NM, Praet SF, Nicolay K, van Loon LJ, Prompers JJ. Early or advanced stage type 2 diabetes is not accompanied by in vivo skeletal muscle mitochondrial dysfunction. Eur J Endocrinol. 2008;158(5):643–53. [PubMed: 18426822]
17. Nabuurs C, Huijbregts B, Wieringa B, Hilbers CW, Heerschap A. 31P saturation transfer spectroscopy predicts differential intracellular macromolecular association of ATP and ADP in skeletal muscle. J Biol Chem. 2010;285(51):39588–96. [PubMed: 20884612]
18. Balaban RS, Koretsky AP. Interpretation of ^{31}P NMR saturation transfer experiments: what you can’t see might confuse you. Focus on “Standard magnetic resonance-based measurements of the Pi→ATP rate do not index the rate of oxidative phosphorylation in cardiac and skeletal muscles”. Am J Physiol Cell Physiol. 2011;301(1):C12–5. [PubMed: 21490314]
19. Gabr RE, Weiss RG, Bottomley PA. Correcting reaction rates measured by saturation-transfer magnetic resonance spectroscopy. J Magn Reson. 2008;191(2):248–58. [PubMed: 18226939]
20. Spencer RG, Fishbein KW, Galban CJ. Pitfalls in the measurement of metabolite concentrations using the one-pulse experiment in in Vivo NMR: commentary on “On neglecting chemical exchange effects when correcting in vivo (31)P MRS data for partial saturation”. J Magn Reson. 2001;149(2):251–7. [PubMed: 11318625]
21. Ren J, Yang B, Sherry AD, Malloy CR. Exchange kinetics by inversion transfer: Integrated analysis of the phosphorus metabolite kinetic exchanges in resting human skeletal muscle at 7 T. Magn Reson Med. 2015;73(4):1359–69. [PubMed: 24733433]
22. Ren J, Sherry AD, Malloy CR. A simple approach to evaluate the kinetic rate constant for ATP synthesis in resting human skeletal muscle at 7 T. NMR Biomed. 2016;29(9):1240–8. [PubMed: 25943328]
23. Ren J, Sherry AD, Malloy CR. Amplification of the effects of magnetization exchange by 31P band inversion for measuring adenosine triphosphate synthesis rates in human skeletal muscle. Magn Reson Med 2015;74(6):1505–14. [PubMed: 25469992]
24. Ren J, Sherry AD, Malloy CR. 31P-MRS of healthy human brain: ATP synthesis, metabolite concentrations, pH, and T1 relaxation times. NMR Biomed. 2015;28(11):1455–62. [PubMed: 26404723]
25. Ren J, Sherry AD, Malloy CR. Band inversion amplifies 31P-31P nuclear Overhauser effects: Relaxation mechanism and dynamic behavior of ATP in the human brain by 31P MRS at 7 T. Magn Reson Med. 2017;77(4):1409–1418. [PubMed: 27060982]
26. Ren J, Sherry AD, Malloy CR. Efficient 31P band inversion transfer approach for measuring creatine kinase activity, ATP synthesis, and molecular dynamics in the human brain at 7 T. Magn Reson Med. 2017;78(5):1657–1666. [PubMed: 27868234]
27. Pouymayou B, Buehler T, Kreis R, Boesch C. Test-retest analysis of multiple 31P magnetization exchange pathways using asymmetric adiabatic inversion. Magn Reson Med. 2017;78(1):33–39. [PubMed: 27455454]

28. Lim EL, Hollingsworth KG, Thelwall PE, Taylor R. Measuring the acute effect of insulin infusion on ATP turnover rate in human skeletal muscle using phosphorus-31 magnetic resonance saturation transfer spectroscopy. NMR Biomed. 2010;23(8):952–7. [PubMed: 20623795]
29. Jelenc MT, Chmelík M, Bogner W, Kršňák M, Trattnig S, Valkovič L. Feasibility and repeatability of localized (31) P-MRS four-angle saturation transfer (FAST) of the human gastrocnemius muscle using a surface coil at 7 T. NMR Biomed. 2016;29(1):57–65. [PubMed: 26684051]
30. Prompers JJ, Wessels B, Kemp GJ, Nicolay K. Mitochondria: investigation of in vivo muscle mitochondrial function by 31P magnetic resonance spectroscopy. Int J Biochem Cell Biol. 2014;50:67–72. [PubMed: 24569118]
31. Parasoglou P, Xia D, Chang G, Regatte RR. 3D-mapping of phosphocreatine concentration in the human calf muscle at 7 T: comparison to 3 T. Magn Reson Med. 2013;70(6):1619–25. [PubMed: 23390003]
32. Bottomley PA, Ouwerkerk R, Lee RF, Weiss RG. Four-angle saturation transfer (FAST) method for measuring creatine kinase reaction rates in vivo. Magn Reson Med. 2002;47(5):850–63. [PubMed: 11979563]
33. Valkovič L, Bogner W, Gajdošík M, Považan M, Kukurová IJ, Kršňák M, Gruber S, Frollo I, Trattnig S, Chmelík M. One-dimensional image-selected in vivo spectroscopy localized phosphorus saturation transfer at 7T. Magn Reson Med. 2014;72(6):1509–15. [PubMed: 24470429]
34. Valkovič L, Chmelík M, Just Kukurova I, Kršňák M, Gruber S, Frollo I, Trattnig S, Bogner W. Time-resolved phosphorous magnetization transfer of the human calf muscle at 3 T and 7 T: a feasibility study. Eur J Radiol. 2013;82(5):745–51. [PubMed: 22154589]
35. Raichle ME, Gusnard DA. Appraising the brain's energy budget. Proc Natl Acad Sci U S A. 2002;99(16):10237–9. [PubMed: 12149485]
36. Bogdanova A, Petrushanko IY, Hernansanz-Agustín P, Martínez-Ruiz A. "Oxygen Sensing" by Na,K-ATPase: These Miraculous Thiols. Front Physiol. 2016 8 2;7:314. [PubMed: 27531981]
37. El-Sharkawy AM, Schär M, Ouwerkerk R, Weiss RG, Bottomley PA. Quantitative cardiac 31P spectroscopy at 3 Tesla using adiabatic pulses. Magn Reson Med. 2009;61(4):785–95. [PubMed: 19195018]
38. Kan HE, Klomp DW, Wong CS, Boer VO, Webb AG, Luijten PR, Jeneson JA. In vivo 31P MRS detection of an alkaline inorganic phosphate pool with short T1 in human resting skeletal muscle. NMR Biomed. 2010;23(8):995–1000. [PubMed: 20878975]
39. Sleigh A, Savage DB, Williams GB, Porter D, Carpenter TA, Brindle KM, Kemp GJ. 31P magnetization transfer measurements of Pi→ATP flux in exercising human muscle. J Appl Physiol (1985). 2016;120(6):649–56. [PubMed: 26744504]
40. Kan HE, Veltien A, Arnts H, Nabuurs CI, Luijten B, de Haan A, Wieringa B, Heerschap A. Gated dynamic 31P MRS shows reduced contractile phosphocreatine breakdown in mice deficient in cytosolic creatine kinase and adenylate kinase. NMR Biomed. 2009;22(5):523–31. [PubMed: 19156695]
41. Nabuurs CI, Choe CU, Veltien A, Kan HE, van Loon LJ, Rodenburg RJ, Matschke J, Wieringa B, Kemp GJ, Isbrandt D, Heerschap A. Disturbed energy metabolism and muscular dystrophy caused by pure creatine deficiency are reversible by creatine intake. J Physiol. 2013;591(2):571–92. [PubMed: 23129796]
42. Ryan TE, Erickson ML, Verma A, Chavez J, Rivner MH, Mccully KK. Skeletal muscle oxidative capacity in amyotrophic lateral sclerosis. Muscle Nerve. 2014;50(5):767–74. [PubMed: 24616062]
43. Bogner W, Chmelik M, Schmid AI, Moser E, Trattnig S, Gruber S. Assessment of (31)P relaxation times in the human calf muscle: a comparison between 3 T and 7 T in vivo. Magn Reson Med. 2009;62(3):574–82. [PubMed: 19526487]

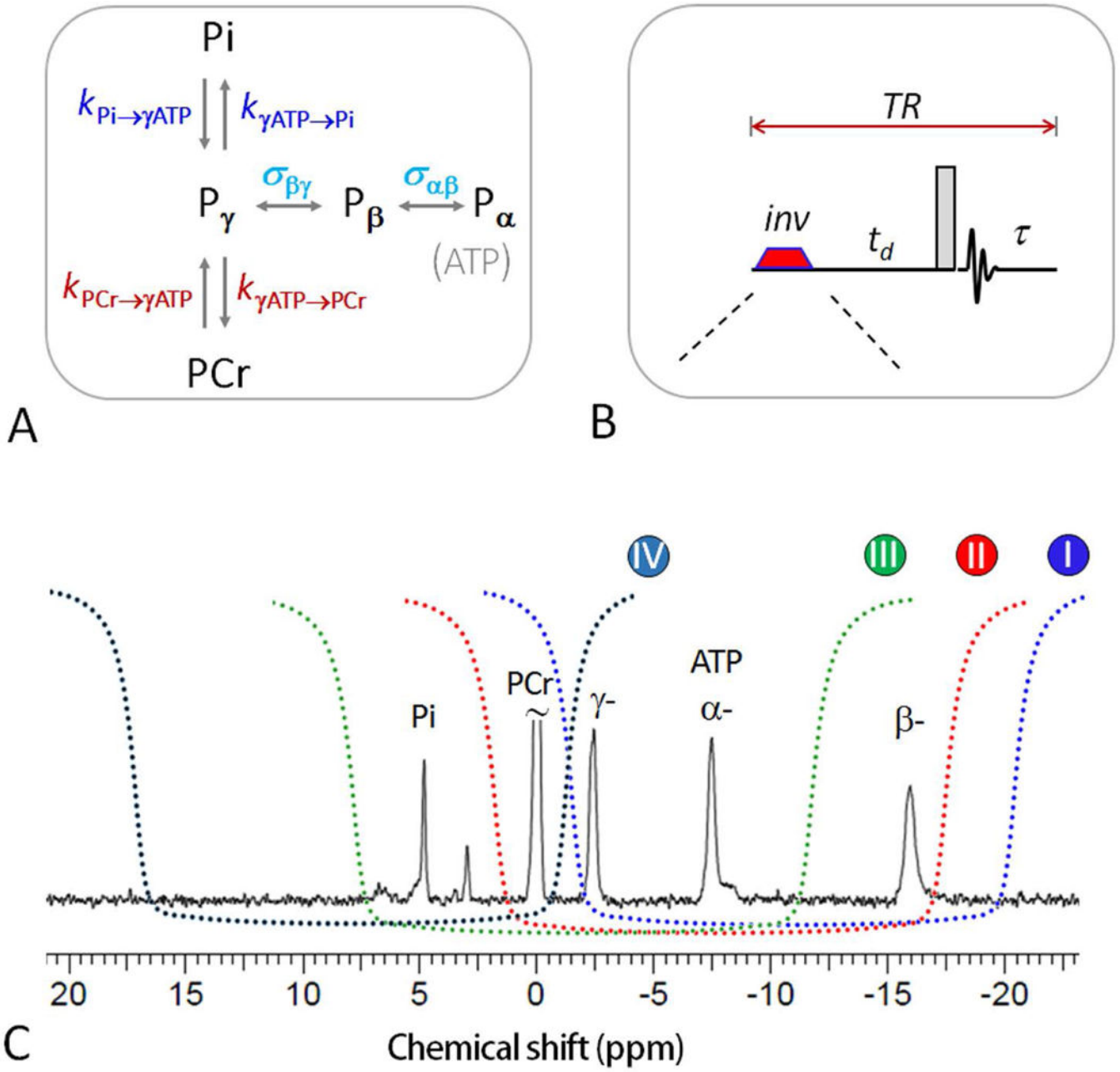

Figure 1.

(A) ^{31}P magnetization exchange system in skeletal muscle, showing various pathways that contribute to the magnetization transfer effects, including kinetic chemical exchange Pi → γ-ATP responsible for de novo ATP synthesis, kinetic chemical exchange PCr → γ-ATP catalyzed by creatine kinase (CK), and ATP intramolecular ^{31}P-^{31}P cross-relaxation γ-(α-) ↔ β-ATP, responsible for the nuclear Overhauser effect; (B) The mEBIT band inversion sequence consists of an adiabatic inversion pulse, followed by a varying delay t_d, a hard readout pulse and FID sampling and magnetization recovery period τ (≈ TR – t_d); and (C) the inversion profile of the three band inversion modules over a brain ^{31}P spectrum. Abbreviation: Pi, inorganic phosphate; PCr, phosphocreatine; ATP, adenosine triphosphate.

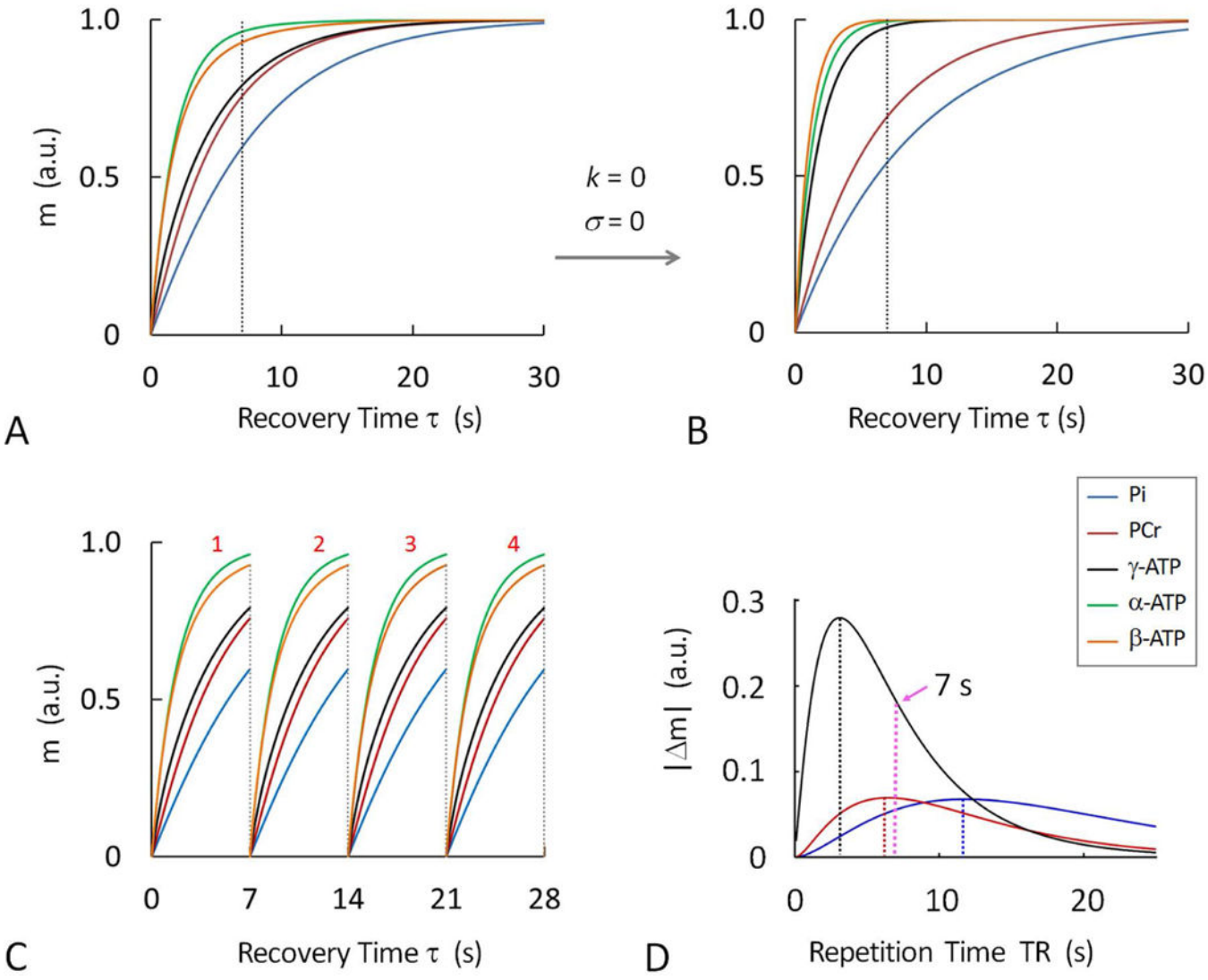

Figure 2.

Simulated ^{31}P magnetizations at varying post-readout recovery time τ, showing the difference in magnetization recovery at Pi, PCr, α-, β- and γ-ATP in the presence (A and C) and absence (B) of chemical exchanges and cross-relaxation, as defined in Figure 1A; (C) Magnetization recovery curves illustrating that short-TR averaging can improve signal-to-noise ratio. (D) Magnetization difference (Δm) between presence and absence of MT effect showing that TR can be optimized to maximally capture MT effects while achieving scan efficiency (calculated optimal TR = 11.6 s for Pi, 6.5 s for PCr and 3.0 s for γ-ATP). The magnetization curves were simulated according to 5-spin exchange model (Figure 1A) and similar k, σ and T_1 values as given in Table 1. Abbreviation: Pi, inorganic phosphate; PCr, phosphocreatine; ATP, adenosine triphosphate.

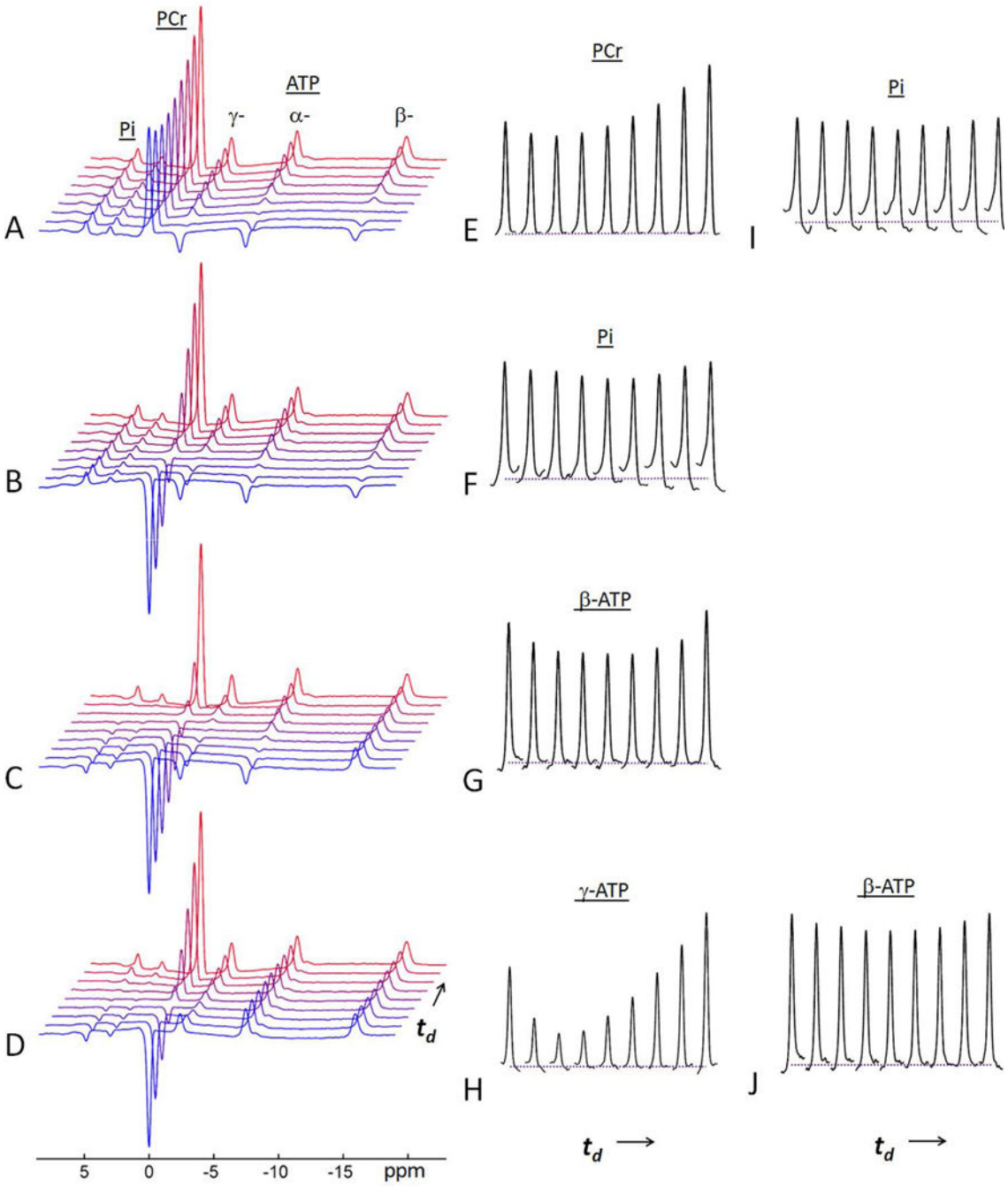

Figure 3.

A representative set of ^{31}P MR spectra acquired from resting skeletal muscle of a 30-year old female subject at 7T using mEBIT modules at constant TR = 7 s and varying inversion delay time t_d. (A, E, and I) data from Module-I; (B and F) data from Module-II; (C and G) data from Module-III; and (D, H and J) data from Module-IV. Note the MT effects at un-inverted spins are manifested as a characteristic "fall-rise" biphasic pattern. The last trace of the spectral series represent the spectrum collected at TR = 7 sec without inversion. For each t_d data series, a total of 7 delay times were sampled, they were spaced logarithmically. The

first t_d point was 30 ms for all modules, while the last t_d was 3 s for Module III, 5 s for Modules I and IV; and 6 s for Module II (see Figure 4 for t_d points).

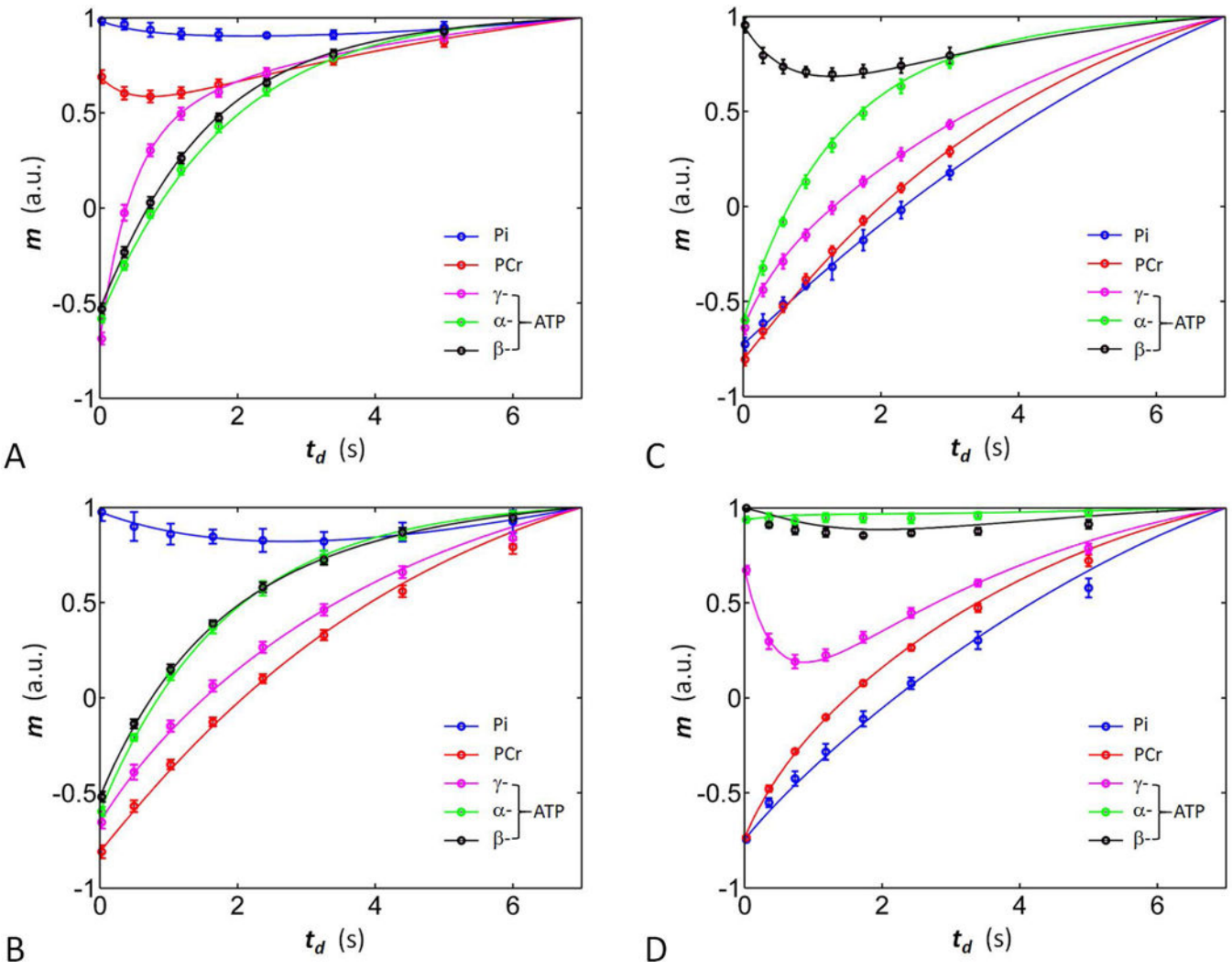

Figure 4.

Plots of the normalized ^{31}P magnetizations versus inversion delay t_d. The solid curves represent the results of simultaneous fitting according to the 5-spin exchange model using datasets obtained from all four modules studied (n = 7 subjects). (A) Module-I; (B) Module-II; (C) Module-III); and (D) Module-IV.

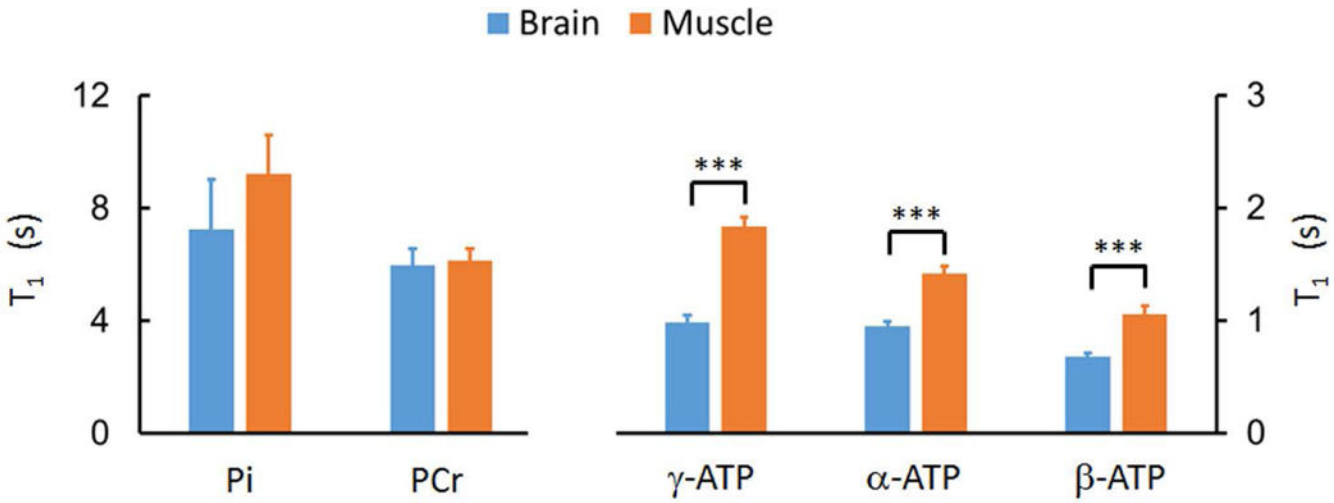

Figure 5.

Comparison of Pi, PCr, and ATP T_1 values between brain and resting skeletal muscle, showing much slower ATP T_1 relaxation in resting muscle than in brain. The symbol "***" indicates $p < 0.001$. The brain ^{31}P T_1 data were from Ren et al (26), evaluated by Module I, II & III with TR = 4 s.

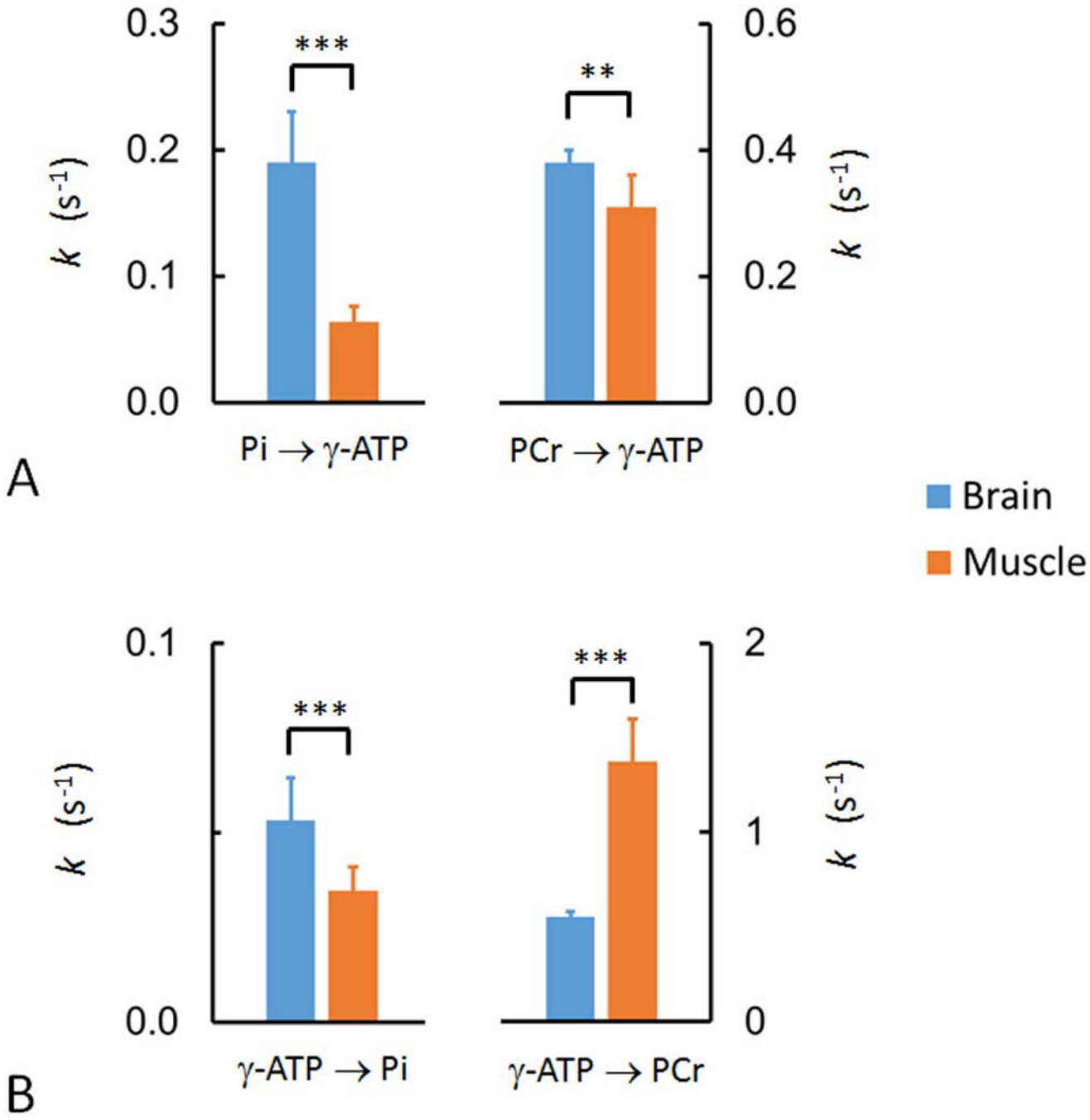

Figure 6.

Comparison of the forward (A) and reverse (B) exchange rate constants between brain and resting skeletal muscle, showing that the turnover rates of Pi and PCr in forward reactions Pi → γ-ATP and PCr → γ-ATP are faster in brain than in muscle. The turnover of ATP in reverse reaction γ-ATP → Pi is also faster in brain than in muscle, whareas the opposite is true for CK-mediated reverse reaction PCr → γ-ATP. Note that, mathematically, $k_{\gamma ATP \rightarrow Pi}$ (= $k_{Pi \rightarrow \gamma ATP}$ [Pi] / [ATP]) reflects de novo ATP synthesis flux normalized to ATP pool size. Similarly, $k_{\gamma ATP \rightarrow PCr}$ (= $k_{PCr \rightarrow \gamma ATP}$ [PCr] / [ATP]) is the normalized ATP synthesis flux

catalyzed by CK. The symbols “**” and “***” denote p-value less than 0.01 and 0.001, respectively. The brain data were from Ren et al (26), evaluated by mEBIT Module I, II & III with TR = 4 s.

Table 1.

mEBIT modules and the corresponding inversion profiles, targeted MT pathways and inversion fractions on ^{31}P resonances.

Modules	Inverted Spins	Un-inverted Spins	Targeted MT Pathways	Inversion Fraction (f)[a]
I	α-, β-, γ-ATP	PCr, Pi	PCr (Pi) → γ-ATP	α-, β-, γ-ATP: −0.58, −0.53, −0.69
II	PCr, α-, β-, γ-ATP	Pi	Pi → γ-ATP	PCr, α-, β-, γ-ATP: −0.81, −0.59, −0.52, −0.65
III	Pi, PCr, α-, γ-ATP	β-ATP	γ (α) ↔ β-ATP	Pi, PCr, α-, γ-ATP: −0.72, −0.81, −0.60, −0.64
IV	Pi, PCr	γ-, α-, β-ATP	γ-ATP→ PCr(Pi), β ↔ γ-ATP	Pi, PCr: −0.74, −0.73

[a]: The variation in inversion fraction f among different ^{31}P resonances is due to its T_2 dependence.

Table 2.

The 7T ^{31}P relaxation time (T_1), and rate constants of kinetic exchanges (k) and cross-relaxation (σ) obtained for the human skeletal muscle at rest by mEBIT

	Band Inversion Modules					
	II	**I & IV**	**I, II & IV**	**I, II & III**	**I, II, III & IV**	**Refs**
K or σ, (s^{-1})						
Pi → γ-ATP	0.083 ± 0.022	0.060 ± 0.026	0.067 ± 0.015	0.065 ± 0.014	0.064 ± 0.012	0.050[a],0.073[b],0.066[c],0.11[d]
PCr → γ-ATP	[0] [h]	0.33± 0.04	0.32± 0.04	0.31 ± 0.05	0.31 ± 0.05	0.26[a],0.25[c],0.29[e],0.31[f],0.34[d]
α(γ)-↔β-ATP [i]	[0] [h]	−0.29 ± 0.05	−0.27 ± 0.05	−0.20 ± 0.02	−0.20 ± 0.03	−0.17[a],0.32[c],1.00[c]
T_1, (s)						
Pi	8.21 ± 2.03	9.11 ± 2.03	9.08 ± 1.58	9.19 ± 1.60	9.24 ± 1.35	7.34[a],6.93[b],8.1[c],6.3[g]
PCr	5.30 ± 0.18	6.79 ± 0.52	6.49 ± 0.46	6.09 ± 0.28	6.15 ± 0.41	5.30[a],6.8[c],4.0[g]
γ-ATP	4.83 ± 0.42	1.61 ± 0.14	1.65± 0.17	1.83 ± 0.12	1.84± 0.08	1.70[a],4.07[b],2.0[c],3.3[g]
α-ATP	1.89 ± 0.08	1.23 ± 0.07	1.28 ± 0.10	1.40 ± 0.08	1.42 ± 0.06	1.30[a], 1.2[c], 1.8[g]
β-ATP	1.92 ± 0.10	0.90 ± 0.08	0.92 ± 0.10	1.04 ± 0.06	1.06 ± 0.07	1.13[a], 0.6[c], 1.8[g]

a: From Ren et al (21) by EKIT with frequency sweeping and 5-pool model at 7T;

b: From Ren et al (23) by EBIT with TR = 30 s and 2-pool exchange model at 7T;

c: From Pouymayou et al (27) by a single module inversion of α-, β- and γ-ATP in thigh muscle at 3T.

d: From Valkovic et al (34) by ST with TR = 15 s, 2-pool exchange model, and $T_{1,app}$ measured under constant irradiation at γ-ATP at 7T (Pi: 3.5 s, and PCr: 1.54 s);

e: From Bottomley et al (32) by Four-Angle Saturation Transfer (FAST) at 1.5T.

f: From Parasoglou et al (31) using continuous ST and IR T_1 measurement at 3T.

g: From Bogner et al (42) by IR with TR = 30 s at 7T, data fitted assuming $k = \sigma = 0$;

h: value in square bracket indicates a fixed constant in data fitting.

i: It was assumed that $\sigma_{\alpha \leftrightarrow \beta\text{-ATP}} = \sigma_{\gamma \leftrightarrow \beta\text{-ATP}}$ (see ref (21)).